

Non-Fermi-Liquid Behavior of Superconducting SnH_4

Ivan A. Troyan, Dmitrii V. Semenok,* Anna G. Ivanova, Andrey V. Sadakov, Di Zhou,* Alexander G. Kvashnin, Ivan A. Kruglov, Oleg A. Sobolevskiy, Marianna V. Lyubutina, Dmitry S. Perekalin, Toni Helm, Stanley W. Tozer, Maxim Bykov, Alexander F. Goncharov, Vladimir M. Pudalov, and Igor S. Lyubutin*

The chemical interaction of Sn with H_2 by X-ray diffraction methods at pressures of 180–210 GPa is studied. A previously unknown tetrahydride SnH_4 with a cubic structure (*fcc*) exhibiting superconducting properties below $T_C = 72$ K is obtained; the formation of a high molecular $\text{C2}/m\text{-SnH}_{14}$ superhydride and several lower hydrides, *fcc* SnH_2 , and $\text{C2-Sn}_{12}\text{H}_{18}$, is also detected. The temperature dependence of critical current density $J_C(T)$ in SnH_4 yields the superconducting gap $2\Delta(0) = 21.6$ meV at 180 GPa. SnH_4 has unusual behavior in strong magnetic fields: *B*, *T*-linear dependences of magnetoresistance and the upper critical magnetic field $B_{C2}(T) \propto (T_C - T)$. The latter contradicts the Wertheimer–Helfand–Hohenberg model developed for conventional superconductors. Along with this, the temperature dependence of electrical resistance of *fcc* SnH_4 in non-superconducting state exhibits a deviation from what is expected for phonon-mediated scattering described by the Bloch–Grüneisen model and is beyond the framework of the Fermi liquid theory. Such anomalies occur for many superhydrides, making them much closer to cuprates than previously believed.

1. Introduction

The study of high-temperature superconductivity is one of the most important problems in condensed matter physics. Compressed polyhydrides are promising high-temperature superconductors, which can be obtained at pressures of 1–2 Mbar. Since 2015, many remarkable hydride superconductors have been experimentally discovered. These are H_3S (with $T_C = 200$ K),^[1] LaH_{10} ($T_C = 250$ K),^[2,3] ThH_9 ($T_C = 146$ K), ThH_{10} ($T_C = 161$ K),^[4] YH_6 ($T_C = 226$ K),^[5,6] and YH_9 ($T_C = 243$ K),^[6] CeH_9 and CeH_{10} ($T_C = 110$ – 120 K),^[7] CaH_6 ($T_C = 215$ K).^[8,9] Most of the superconducting polyhydrides contain elements of groups IIIA, IVB with d^0 - $d(f)^1$ valent electrons,^[10] whereas polyhydrides of *p*-elements, and in particular Sn, have not been studied enough.

In the last 10 years, the chemistry of polyhydrides of group IV elements (C, Si,

I. A. Troyan, A. G. Ivanova, M. V. Lyubutina, I. S. Lyubutin
Shubnikov Institute of Crystallography
Federal Scientific Research Center Crystallography and Photonics
Russian Academy of Sciences
59 Leninsky Prospekt, Moscow 119333, Russia
E-mail: lyubutinig@mail.ru

D. V. Semenok, D. Zhou
Center for High Pressure Science and Technology Advanced Research (HPSTAR)
Beijing 100193, China
E-mail: dmitrii.semenok@hpstar.ac.cn; di.zhou@hpstar.ac.cn

A. V. Sadakov, O. A. Sobolevskiy, V. M. Pudalov
V. L. Ginzburg Center for High-Temperature Superconductivity and Quantum Materials P. N. Lebedev Physical Institute
Russian Academy of Sciences
Moscow 119991, Russia

A. G. Kvashnin
Skolkovo Institute of Science and Technology
Bolshoy Boulevard, 30/1, Moscow 121205, Russia

I. A. Kruglov
Center for Fundamental and Applied Research
Dukhov Research Institute of Automatics (VNIIA)
st. Sushchevskaya, 22, Moscow 127055, Russia


I. A. Kruglov
Laboratory of Computational Materials Discovery
Moscow Institute of Physics and Technology
9 Institutsky Lane, Dolgoprudny 141700, Russia

D. S. Perekalin
A.N. Nesmeyanov Institute of Organoelement Compounds
Russian Academy of Sciences
28 Vavilova str., Moscow 119334, Russia

T. Helm
Hochfeld-Magnetlabor Dresden (HLD-EMFL) and Würzburg-Dresden Cluster of Excellence
Helmholtz-Zentrum Dresden-Rossendorf (HZDR)
01328 Dresden, Germany

S. W. Tozer
National High Magnetic Field Laboratory
Florida State University
Tallahassee, Florida 32310, USA

M. Bykov
Institute of Inorganic Chemistry
University of Cologne
50939 Cologne, Germany

 The ORCID identification number(s) for the author(s) of this article can be found under <https://doi.org/10.1002/advs.202303622>

© 2023 The Authors. Advanced Science published by Wiley-VCH GmbH. This is an open access article under the terms of the Creative Commons Attribution License, which permits use, distribution and reproduction in any medium, provided the original work is properly cited.

DOI: 10.1002/advs.202303622

Ge, Sn, Pb) has been intensively studied by means of the density functional theory (DFT). The experimental synthesis of such polyhydrides is carried out at high-pressure in diamond anvil cells (DACs). C, Si, and Ge hydrides are mainly low-symmetry molecular covalent compounds with moderate superconducting properties^[11–13]. The higher molecular silicon polyhydride $\text{SiH}_4(\text{H}_2)_2$ was observed in experiments of Strobel et al. and Wang et al.^[14,15] Resistive transitions with T_C up to 79 K for silicon polyhydrides were obtained under high pressure by the group of M. Eremets et al.^[16] Theoretical calculations for Ge hydrides at 200–300 GPa, predicted stable low symmetry phases of GeH_3 and Ge_3H_{11} , and various polymorphic modifications of the well-known GeH_4 .^[13,17] A new molecular compound, possibly $\text{GeH}_4(\text{H}_2)_2$, was obtained experimentally at 7.5 GPa.^[18] According to theoretical calculations, metallic $P2_1/c\text{-GeH}_4(\text{H}_2)_2$ is a superconductor with T_C of 76–90 K at 250 GPa.^[19]

The increase in metallicity of Sn to Pb results in the appearance of thermodynamically stable polyhydrides in the high-pressure phase diagram. For instance, theory predicts the formation of $C2/m\text{-SnH}_{12}$, $C2/m\text{-SnH}_{14}$,^[20] and various PbH_4 , PbH_6 , and PbH_8 ^[21–23] lead polyhydrides under high pressure. However, attempts to synthesize Pb polyhydrides have been unsuccessful to date.^[24] The recent observation by Hong et al.^[25] of a sharp drop in electrical resistance in unidentified Sn polyhydride at 71 K motivated us to investigate in detail the structure and superconducting properties of Sn polyhydrides under high pressure.

Three series of XRD experiments were carried out at different synchrotron facilities such as European Radiation Synchrotron Facility (ESRF) in 2017, Positron-Electron Tandem Ring Accelerator (PETRA) in 2020 and Advanced Photon Source (APS) in 2022. At pressures around 160–210 GPa, we observed X-ray diffraction patterns of the studied samples, which are attributed to different Sn hydrides formed. Most X-ray diffraction (XRD) patterns have a characteristic set of cubic ($Fm\bar{3}m$) reflections. In the experiment performed at APS, a single-crystal XRD at a pressure of ≈ 190 GPa was carried out. An analysis of the diffraction pattern confirmed the cubic structure ($Fm\bar{3}m$) of the Sn sublattice in SnH_4 . As we have found, tin tetrahydride is a non-Fermi liquid metal, which demonstrates anomalous behavior of electrical resistance, T -linear upper critical magnetic field, and H -linear magnetoresistance in a wide range of temperatures and magnetic fields.

2. Results

2.1. High-Pressure Synthesis of SnH_4 with a Cubic (fcc) Structure

In this work, tin polyhydrides were synthesized and studied by X-ray diffraction. The previously unknown tetrahydride SnH_4

with a cubic structure (fcc) was synthesized at high pressures in diamond anvil cells in two different ways. In the first approach, we used the reaction of solutions of SnCl_4 and LiAlH_4 . Gaseous stannane SnH_4 was emanated, then condensed upon cooling with liquid nitrogen.^[26] Using a cryogenic filling at a pressure of ≈ 2.0 bar, liquefied SnH_4 was supplied through a thin capillary into the working volume of the DAC, and then compressed to high pressure at room temperature (Figure S7, Supporting Information). Monitoring the successful loading of gaseous SnH_4 and its compression provided additional confirmation of the hydrogen content in the resulting high-pressure phase fcc SnH_4 . In the second approach, SnH_4 was synthesized during the interaction of pre-compressed piece of metallic Sn and hydrogen produced by laser heating of NH_3BH_3 under high pressure. A table summarizing all the performed experiments can be found in the Tables S1 and S5 (Supporting Information).

Let us first consider the results of the initial experiment we performed at the ID27 beamline of ESRF in 2017 (Figure 1). Our preliminary study of the compression of pure Sn (Figure 1a, DAC S1) showed that at 190 GPa it exists in two modifications: hexagonal (hcp) and cubic (bcc), the latter one is dominant. In fact, the phase transition $bcc \rightarrow hcp$ starts already at 160 GPa.^[27] However, the enthalpies of formation of these modifications differ very little (according to DFT calculations it is $\Delta H = 9.5$ meV per atom), which explains the very low rate of this transformation. As follows from the XRD pattern in Figure 1a, at 190 GPa, the Sn unit cell volume is $V(\text{Im}\bar{3}m\text{-Sn}) = 26.9 \text{ \AA}^3$, which agrees with results of a previous publication.^[28] Interesting, but the unit cell volumes of hcp Sn and bcc Sn are very similar.

During the experiment with stannane, frozen SnH_4 was placed in DAC S2 and compressed to 180 GPa. It was found that with an increase in pressure, rapid metallization of SnH_4 occurs at ≈ 10 GPa (Figure S9, Supporting Information), accompanied by the disappearance of the Raman signal. At ≈ 160 GPa, a new cubic modification of SnH_4 is formed. Figure 1b shows that the Bragg peaks of the experimental XRD patterns of SnH_4 at pressures 160–180 GPa are best indexed by a face-centered cubic lattice (fcc) with unit cell volume $19.6 \text{ \AA}^3/\text{Sn}$ at 180 GPa. The obtained XRD patterns also contain an impurity (broadened peaks at $2\theta = 9.5^\circ$ and 10.2°) which can be attributed to hcp Sn formed during SnH_4 dissociation when loaded and compressed in the DAC S2. Stannane is thermodynamically unstable and under ambient conditions it gradually decomposes to Sn and H_2 .

Compressed Sn hydrides were also experimentally studied by Hong et al.^[25] The authors obtained a similar X-ray diffraction pattern (Figure 1d, the only XRD pattern in Ref. [25]), indexed as $C2/m\text{-SnH}_{12}$ ($a = 5.179 \text{ \AA}$, $b = 3.038 \text{ \AA}$, $c = 7.364 \text{ \AA}$, $\beta = 149.11^\circ$). This structure was previously predicted by DFT methods.^[20] It can be seen that the experimental XRD clearly does not match the theoretically predicted XRD of SnH_{12} (black curve in Figure 1d). At the same time, the experimental XRD pattern (blue curve in Figure 1d) fits well with the theoretical model of fcc SnH_4 , namely $Fd\bar{3}m\text{-Sn}_8\text{H}_{30}$ ($= \text{SnH}_{3.75}$, red curve in Figure 1d), which is discussed in details in the Supporting Information (“Crystal structure search” section). The unit cell volume of the Sn_8H_{30} is $V = 19.64 \text{ \AA}^3/\text{Sn}$ (or 628.68 \AA^3 for $Z = 32$) at 180 GPa. Using the data obtained in the ESRF-2017 experiment, we refined unit cell parameters of $Fd\bar{3}m\text{-Sn}_8\text{H}_{30}$, which were found to be in a good

A. F. Goncharov
Earth and Planets Laboratory
Carnegie Institution for Science
5241 Broad Branch Road NW, Washington, DC 20015, USA

V. M. Pudalov
HSE Tikhonov Moscow Institute of Electronics and Mathematics
National Research University Higher School of Economics
20 Myasnitckaya ulitsa, Moscow 101000, Russia

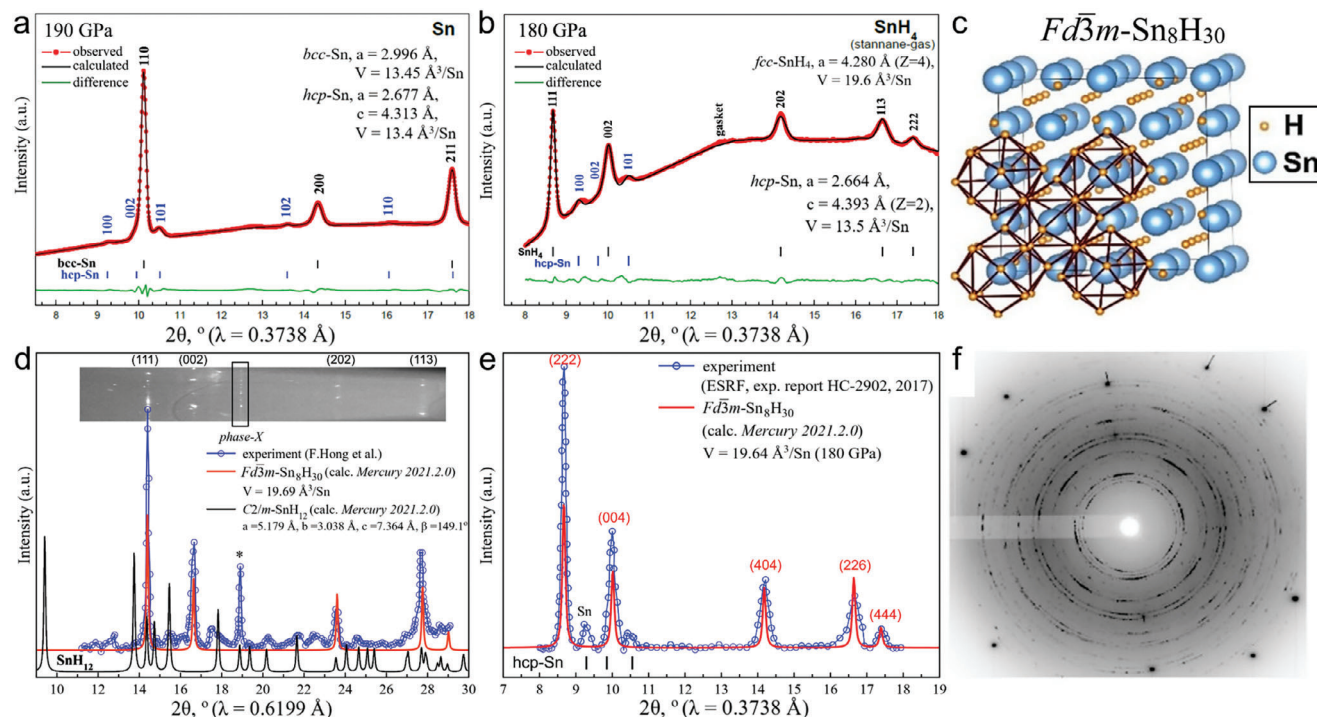


Figure 1. X-ray diffraction patterns and the Le Bail refinements of the unit cell parameters of a) Sn at 190 GPa in DAC S1, and b) SnH₄ and hcp Sn obtained after compression of gaseous stannane to 180 GPa in DAC S2 (ESRF-2017). c) The crystal structure of theoretical model, $Fd\bar{3}m$ -Sn₈H₃₀, which best fits the experimental pattern. d) XRD pattern of Sn hydride obtained by Hong et al.^[25] (blue curve, 206 GPa) and its fit by $Fd\bar{3}m$ -Sn₈H₃₀ model (red curve). Asterisk indicate uninterpreted reflection (phase X). Obviously, the diffraction pattern does not correspond to the $C2/m$ -SnH₁₂ structure (black curve) proposed by Hong et al. e) Fitting of the experimental XRD pattern after background subtraction (ESRF-2017) using theoretical model $Fd\bar{3}m$ -Sn₈H₃₀ (red curve) and hcp Sn phase (black dashes). It gives much better result than $C2/m$ -SnH₁₂. f) Typical X-ray diffraction pattern of fcc SnH₄ at 170 GPa (PETRA-2020, DAC D2).

agreement with the results of DFT calculations (Tables S5 and S8, Supporting Information).

2.2. Synthesis of Molecular SnH₁₄

The next experiments were performed at the P02.2 PETRA III beamline in 2020. As has already been shown, stannane compression leads to the formation of mixtures of hcp Sn and cubic SnH₄. This indicates an insufficient amount of hydrogen for the complete conversion of Sn to polyhydrides. Therefore, to obtain tin hydrides with a higher hydrogen content (similar to SrH₂₂³³ and BaH₁₂³⁴), we decided to use ammonia borane NH₃BH₃ (AB) as a source of H₂ in DACs D2 and M2.

The use of AB has yielded interesting results. We found that in addition to SnH₄, several new compounds are formed, whose XRD patterns mostly correspond to the higher molecular polyhydride $C2/m$ -SnH₁₄ predicted in 2016^[29] (Figure 2). The refinements of the unit cell parameters of synthesized SnH₁₄ (Figure 2a,b,d) are in a good agreement with the theoretical DFT calculations (Table S9, Supporting Information).

This polyhydride has an orthorhombic $Immm$ -Sn sublattice and a hydrogen sublattice, consisting of H₂ ($d_{HH} = 0.833$ Å) and H₃ ($d_{HH} = 0.92$ Å) fragments. According to molecular dynamics modeling, $C2/m$ -SnH₁₄ is dynamically stable in the anharmonic approximation (Figure S13, Supporting Information). This is un-

usual for molecular polyhydrides, but SnH₁₄ exhibits the properties of a typical metal with a high density of electronic states at the Fermi level (DOS). The DOS projection on hydrogen atoms, $N_F(H) = 0.32$ states per eV per f.u., is larger than that on Sn atoms ($N_F(Sn) = 0.23$ states per eV per f.u.). The hydrogen sublattice exhibits anisotropic properties, and is in a solid (not glassy, like in $P1$ -SrH₂₂^[30]) state. Due to the presence of large amount of molecular hydrogen in the structure of SnH₁₄, its Debye temperature is rather high ($\theta_D \approx 1500$ K, ω_{log} up to 1250 K). Also, the superconducting properties are well pronounced, the electron-phonon coupling (EPC) coefficient is $\lambda = 1.25$, and the critical temperature is $T_C = 107$ – 133 K at 200 GPa ($\mu^* = 0.15$ – 0.1) in the harmonic approximation (Figures S12 and S13, Supporting Information). This significantly distinguishes molecular tin polyhydrides from similar compounds of barium (BaH₁₂, which is a low- T_C superconductor, $T_C \approx 20$ K) and strontium (SrH₂₂, which is a semiconductor).

In our last experiment performed in 2022 at APS, Sn, and AB were again used. The studies were carried out in DAC S3 with a wide opening angle ($\approx 70^\circ$) and diamond anvils of the Böhler-Almax type to obtain a single-crystal XRD pattern (Figure S2, Supporting Information), where one phase was indexed by the fcc SnH₄ (R -factor is 4.75 %). A co-product of the synthesis is a lower hydride, whose X-ray diffraction pattern can be indexed by $C2$ -Sn₁₂H₁₈ ($=$ Sn₂H₃, $R_1 = 5.83\%$, Figure S4, Supporting Information) with an experimental unit cell volume of 15.85 Å³/Sn

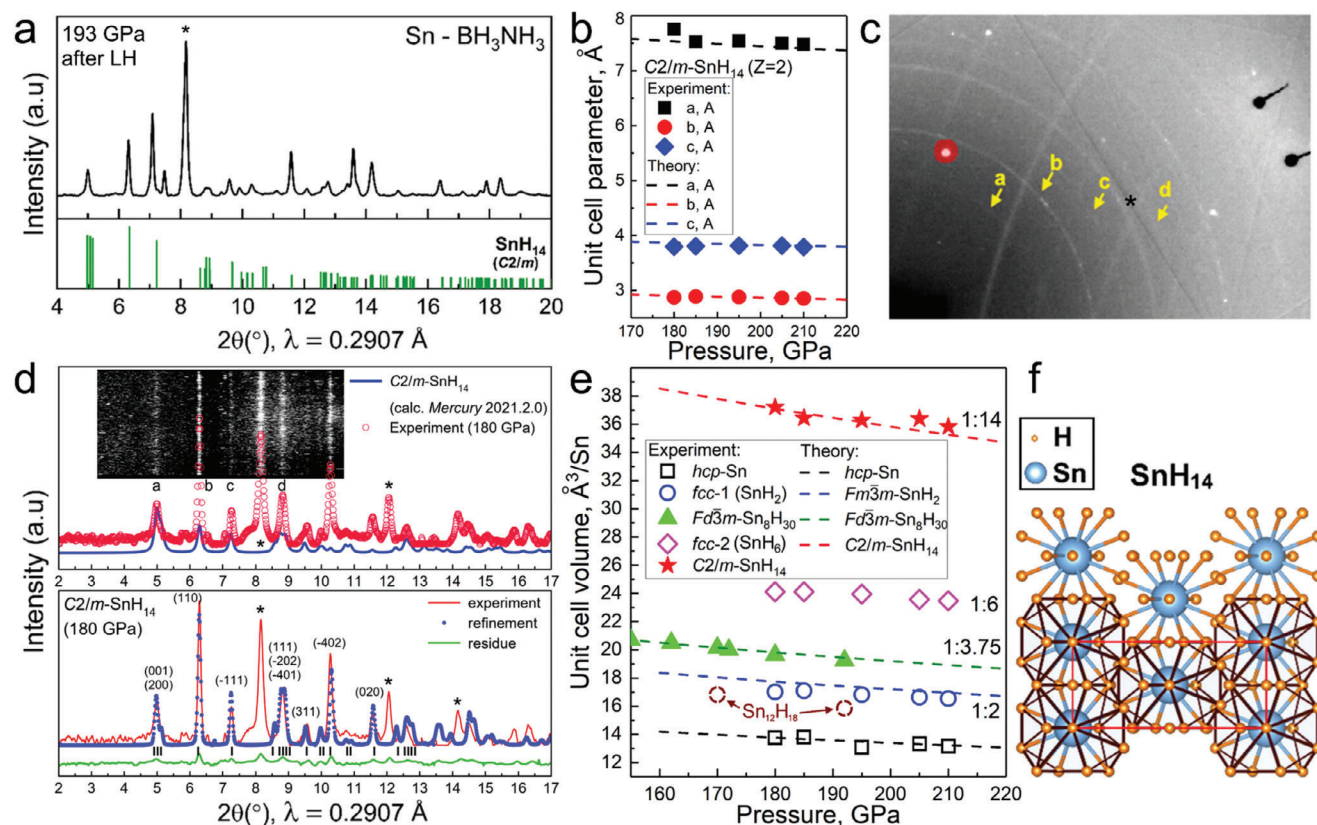


Figure 2. X-ray diffraction patterns and the Le Bail refinements of the unit cell parameters of Sn hydrides in DACs D2 and M2. a) XRD pattern of SnH_x in NH_3BH_3 media after the laser heating at 193 GPa. Predicted XRD of C2/m-SnH_{14} is shown on the bottom panel. b) Experimental and theoretical dependences of the unit cell parameters on the pressure for C2/m-SnH_{14} . c) Typical diffraction pattern at 180 GPa (PETRA-2020, $\lambda = 0.2904 \text{ \AA}$). Asterisks denote uninterpreted peaks, “a–d” denote main reflections from SnH_{14} . d) Comparison of experimental and calculated XRD reflection intensities for SnH_{14} (“a–d”). Inset: diffraction image (“cake”). Bottom panel: the Le Bail refinement of C2/m-SnH_{14} . Unidentified reflections are marked by asterisks. The experimental data, fitted line, and residues are shown in red, blue, and green, respectively. e) Pressure–unit cell parameters diagram for all tin hydrides synthesized in our experiments: stars, rhombuses, triangles, circles, and squares show the experimental data, lines depict the theoretical calculations. f) Crystal structure of SnH_{14} polyhydride.

at 192 GPa. This phase was found during the USPEX crystal structure search. Obtained $\text{Sn}_{12}\text{H}_{18}$ consists of $[\text{SnH}_4]$ structural blocks with $d_{\text{Sn-H}} = 1.87\text{--}1.97 \text{ \AA}$ (at 200 GPa) and multiple Sn–H–Sn hydrogen bonds.

Summarizing the structural studies of tin hydrides at high pressures, we can conclude that the Sn–H system is very rich in various compounds. Structural interpretation of most of these compounds is difficult because of the low enthalpy of formation of Sn hydrides. This does not allow reliable use of computational methods to predict thermodynamically stable phases. Obviously, the main product of the reaction of tin with hydrogen is fcc-SnH_4 ($V = 19.6 \text{ \AA}^3/\text{Sn}$ at 180 GPa). Among the higher polyhydrides C2/m-SnH_{14} ($V = 35.8 \text{ \AA}^3/\text{Sn}$ at 193 GPa) and, possibly, $\text{fcc-SnH}_{6\pm x}$ ($V = 24.1 \text{ \AA}^3/\text{Sn}$ at 180 GPa, $x = 0.5$) were found. Among the lower hydrides fcc-SnH_{2+x} ($V = 17.0 \text{ \AA}^3/\text{Sn}$ at 185 GPa, $x \approx 0.5$) and $\text{C2-Sn}_{12}\text{H}_{18}$ ($V = 15.85 \text{ \AA}^3/\text{Sn}$ at 192 GPa) were synthesized.

2.3. Transport Properties of fcc-SnH_4

Knowing the crystal structure of new hydride compounds, it is very important to experimentally study their physical properties.

Therefore, we studied the transport properties of the obtained fcc-SnH_4 using a four-electrode Van der Pauw circuit sputtered on diamond anvils. At 180 GPa, a sharp drop in the sample electrical resistance (by a factor of 10^3) at $T_C = 72 \text{ K}$ with the width of $\Delta T_C = 2 \text{ K}$ was revealed (Figure 3a). The sample can therefore be characterized as homogeneous, which is also confirmed by the single crystal XRD data. It has been established that in external magnetic fields up to 16 T the value of the critical temperature T_C decreases almost linearly, which is typical for superconductors (Figure 3b,c). In the external magnetic fields (H_{ext}) we observed a significant broadening of superconducting transitions in the range of 2–10 K (Figure 3d), which correlates with data of Ref. [25]. According to previous results,^[31–33] the superconducting transitions of some polyhydrides practically do not broaden in relatively weak magnetic fields ($\mu_0 H_{\text{ext}} < 0.5 B_{C2}(0)$). Here, due to a much lower critical field $B_{C2}(0)$ for SnH_4 we were able to trace the $B_{C2}(T)$ dependence over almost the entire temperature range. As Figure 3b,d show, SnH_4 manifests pronounced broadening of the superconducting transition in external fields.

All of the samples we examined in electrode DACs were superconducting at pressures above 170 GPa. Several SC transitions corresponding to different tin hydrides were observed in

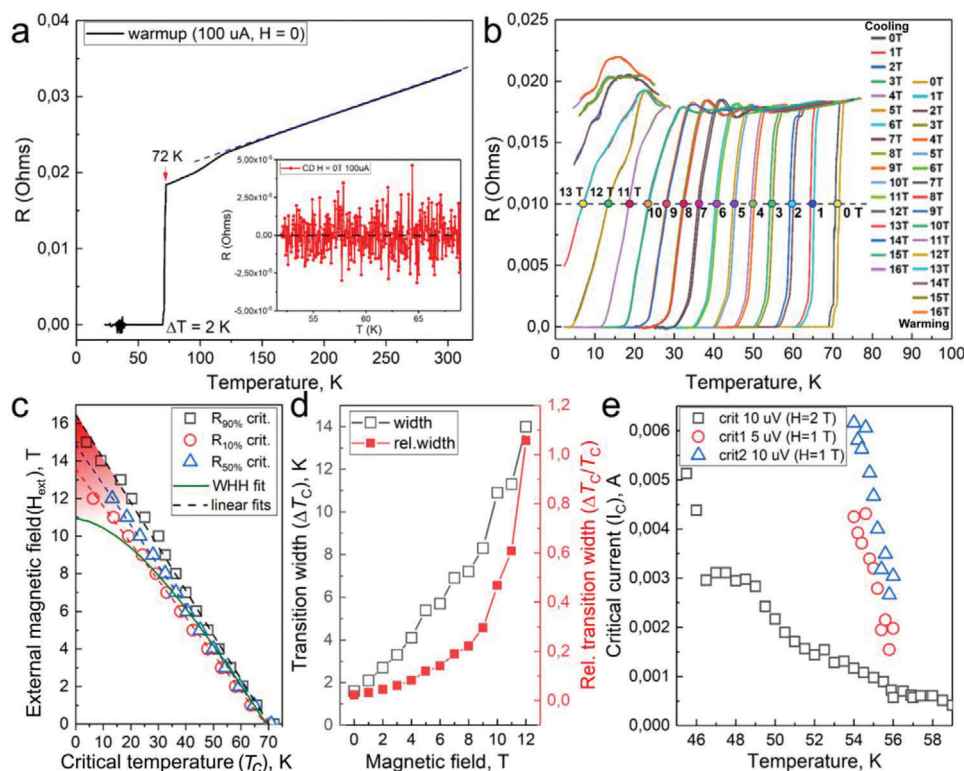


Figure 3. Electric transport properties of *fcc* SnH₄ at 180 GPa studied in magnetic fields. a) Temperature dependence of the electrical resistance of the sample. Fully linear $R(T)$ is observed from 300 to 120 K. At ≈ 30 K, the electrode system becomes unstable. Inset: residual resistance at $T < T_C$. b) Displacement of the superconducting transition in external magnetic fields up to 16 T in warming and cooling cycles. c) Experimental temperature dependence of T_C (H_{ext}). Using linear interpolation by different criteria (90, 50, and 10% of the normal state resistance) the values of upper critical magnetic field (B_{C2}) were obtained. WHH fit is shown with a green curve. The area of deviation from this model is marked in red (see also Figure S24b, Supporting Information). d) Relative and absolute broadening of superconducting transitions in external magnetic fields. e) Temperature dependence of the critical current of the Sn hydride sample in external magnetic fields of 1 and 2 T.

some DACs (see Figures S17 and S18, Supporting Information, T_C 's ≈ 25 and 39 K). The highest T_C observed in the Sn-H system in our experiments is 72–74 K at 180–190 GPa. When the pressure drops below 170 GPa, a sharp decrease in T_C to 20–25 K is found. The superconducting transition temperature in SnH₄ increases with increasing pressure: T_C (180 GPa) = 72 K, T_C (190 GPa) = 74 K, T_C (≈ 200 GPa) = 75 K (warming cycle^[25]). This corresponds to a positive slope $dT_C/dP = +0.1 - 0.2$ K GPa⁻¹, which is expectedly associated with acoustic phonons hardening (Section S7, Supporting Information).

Linear extrapolation of $B_{C2}(T)$ to $T_C = 0$ K allows the upper critical magnetic field of SnH₄ to be estimated as $B_{C2}(0) = 14\text{--}16$ T. This is a very low value compared to other hydride superconductors. For example, YH₆⁵ has the $B_{C2}(0)$ value of at least 110–160 T, and for LaH₁₀² it is at least 140–160 T. One possible reason of that is the relatively low density of electronic states (Figure S11, Supporting Information), in particular, the low contribution of the hydrogen sublattice to the total density of electronic states of SnH₄, which is critical for superconductivity in polyhydrides. Analogies can be found in studies of the cerium CeH₉₋₁₀^[7] and thorium ThH₉₋₁₀^[4] superhydrides which despite higher T_C also exhibit relatively low $B_{C2}(0) \approx 27\text{--}45$ T.

From measurements of the temperature dependence of resistance, we focus first on a pronounced feature (kink) at ≈ 120 K

(Figure 3a; Figures S17b and S18b, Supporting Information) which we observed in several experiments. Hong et al.^[25] also saw a similar kink in the $R(T)$ dependence for SnH₄. Such anomalous behavior of $R(T)$ was previously revealed in many hydrides, for instance, in BaH₁₂,^[34] H₃S^[1] and LaH₁₀,^[2,35] and in cuprates.^[36] Additional examples are given in Figures S20 and S21 (Supporting Information). Second, electrical resistance of SnH₄ is completely linearly dependent on temperature ($\beta = R_0^{-1} dR/dT = 1.77 \times 10^{-3}$ K⁻¹) in the range from 120 to 320 K (see Figure 3a). Because of these two anomalies, the resistance of SnH₄ in the normal (non-superconductive) state can hardly be fitted with the Bloch-Grüneisen model^[37] of phonon-mediated scattering. Indeed, an attempt to use the Bloch-Grüneisen fit^[37] leads to a unrealistically low Debye temperature (θ_D) of ≈ 100 K, which is not typical for polyhydrides under high pressure. A power-law interpolation $R(T) = R_0 + AT^n$ (Figure S22, Supporting Information) commonly used to analyze the Fermi-liquid behavior, also indicates significant deviations in the SnH₄ properties from the behavior of ordinary metals.

The linear dependence of the upper critical field on temperature requires more detailed discussion. For superconductors described by the Bardeen-Cooper-Schrieffer (BCS) theory,^[38] the generally accepted model for the $B_{C2}(T)$ dependence is the Werthamer-Helfand-Hohenberg (WHH) model, which predicts

flattening of the $B_{C2}(T)$ dependence at low temperatures.^[39] However, for many compressed polyhydrides (e.g., YH_4 , LaH_x at low pressure^[40]) the $B_{C2}(T)$ function is almost linear down to temperatures of 1–2 K. Such behavior sometimes may be explained by the presence of two superconducting gaps^[41–44] (Figure S19, Supporting Information). Indeed, for a number of polyhydrides ($\text{Fm}\bar{3}m\text{-LaH}_{10}$, $\text{Fm}\bar{3}m\text{-YH}_{10}$, $\text{P6}_3/\text{mmc-YH}_9$) the solution of the anisotropic Migdal-Eliashberg equations indicates the presence of two superconducting gaps.^[45–47] However, this explanation is unsatisfactory, since two-gaps superconductivity is not universal (e.g., $\text{Im}\bar{3}m\text{-CaH}_6$ ^[48]). Another possible explanation is related to the mesoscopic inhomogeneity of the sample, the presence of regions (“islands”) with different composition and hydrogen content and, consequently, with different T_C and B_{C2} .^[32,49,50] As long as such “islands” of superconductivity are still bound via the Josephson effect, one can still detect the superconductivity of the sample. The proposed explanation agrees with the appearance of an ascending feature in $R(T)$, indicating a significant increase in resistance at low temperatures (Figure 3b), possibly, due to the complex and shunted trajectory of the electric current.

One of the distinguishing features of superconductors is the existence of a critical current density $J_C(T)$, when superconductivity gets destroyed and the electrical resistance of the material becomes nonzero. The low upper critical magnetic field of SnH_4 , as expected, leads to low values of the critical current of the sample: $J_C = 6 \text{ mA}$ at 55 K in a magnetic field of 1 T, that corresponds to $J_C(55 \text{ K}, 1 \text{ T}) \approx 200 \text{ A mm}^{-2}$ for the sample with 1 μm thickness and 30 μm diameter (Figure 3e; Figure S17a, Supporting Information). However, if we consider not the maximum size of the sample, but the interelectrode distance, which for our sputtering mask is $\approx 7 \mu\text{m}$, then the estimates of the critical density increase significantly (see below).

The critical current measurements can be used to estimate the superconducting gap in SnH_4 . Talantsev et al.,^[51,52] proposed the following model for s-wave superconductors

$$J_c(T) = \frac{B_{c1}(T)}{\mu_0 \lambda_L(T)} \quad (1)$$

where $J_C(T)$ is the critical current density at temperature T in the absence of the magnetic field, and $\lambda_L(T)$ is the penetration depth, and $B_{c1}(T)$ – is the lower critical magnetic field. Detailed equations for this model are provided in Equation S5, Supporting Information. Surprisingly, superconductivity in tin hydride is quite easily suppressed by electric current. Fit of experimental $J_C(T)$ data (Figure S17, Supporting Information) yields $2\Delta(0) \approx 21.6 \text{ meV}$ and $2\Delta(0)/k_B T_C = 3.6$, in a reasonable agreement with the BCS value of 3.52. At the same time, according to the Talantsev-Tallon model, the self-field critical current density in SnH_4 at 0 K can reach $J_C(0) = 8.8 \text{ kA mm}^{-2}$. Thus, superconductivity in SnH_4 probably has a conventional electron-phonon mechanism.

The results of studying the magnetoresistance (MR) of SnH_4 at 180 GPa in pulsed magnetic fields up to 65 T revealed a curious result. The dependence of the electrical resistance $\delta R = (R - R_0) \propto \mu^2 B^2$ on magnetic field B_{ext} (where μ is the mobility of carriers)^[53] is quadratic only in relatively weak magnetic fields. Then, rather

quickly (when $B_{\text{ext}} > B_{\text{crit}}$) this dependence becomes linear $\delta R \propto (B - B_0)$, see Figure 4a,c. Taken separately, each of the two effects – linear $\delta R(T)$ and linear $\delta R(B)$ dependences may find analogies in other fields of physics. For example, linear $\delta R(T)$ occurs in strongly interacting 2D systems of electrons^[54] where it originates from interaction assisted impurity scattering. Linear $R(B)$ is known for polycrystalline samples (Kapitza linear magnetoresistance) and originates from scattering by the grain boundaries in quantizing magnetic fields,^[55–57] or is found in materials with Dirac cone spectrum. Mesoscopic disorder with several metal phases can also lead to such effect.^[58] However, the combination of the two effects in one and the same material leaves the most probable only one analogy – with high- T_C cuprates which exhibit non-Fermi-liquid behavior in the normal state.^[59,60] These so called strange metals are known to be materials between insulators and metals.^[61] Following the interpretation widely used for cuprate superconductors, we can say that the combination of the anomalous T and B -linear behavior of electrical resistance and magnetoresistance, as well as the upper critical field of fcc SnH_4 allows to characterize the tin tetrahydride in the normal state as a non-Fermi-liquid strange metal.

In general, the results of experiments in pulse magnetic fields agree with measurements in steady fields below 16 T: the MR of SnH_4 only in the initial part (up to 5–7 T) is a quadratic function of the field. With a further increase in the field, MR becomes completely B -linear. In addition, measurements in weak magnetic fields (0–16 T, at 75–100 K, Figure 4c,f) allowed us only to estimate the Hall coefficient $R_H \approx 5 \times 10^{-12} \text{ m}^3 \text{ C}^{-1}$. The detected Hall voltage was unusually small $\Delta V_H \approx 1\text{--}2 \times 10^{-8} \text{ V}$ at a current of 0.5 mA (Figure 4d). It is impossible to give a more accurate estimate, since we do not know the exact thickness (t) of the sample ($t \approx 1\text{--}2 \mu\text{m}$). Nevertheless, this value of R_H is rather small which allows us to consider the concentration of charge carriers in SnH_4 under pressure to be rather high $10^{29}\text{--}10^{30} \text{ m}^{-3}$ (as $R_H = 1/n_e e$, the sign of the carrier charge is unknown). Alternatively, the low Hall coefficient may be due to high hole mobility, which can make a significant contribution to the conductivity and reduce the Hall coefficient. For instance, rough estimates of the mobility of electrons and holes in Sn_8H_{30} at 180 GPa show that the mobility of holes in tin tetrahydride can be tens of times higher than the electron mobility (Table S14, Supporting Information).

Given the almost identical value of the Fermi velocity $V_F = 2.5 \times 10^5 \text{ m s}^{-1}$ in various hydride superconductors,^[62] we can estimate the mean free path of an electron in SnH_4 in terms of the Drude theory:^[63,64]

$$l_e = V_F \tau \approx \frac{m_e R_H}{e R t} \quad (2)$$

where R is the electrical resistance of the sample. It can be seen that in the SnH_4 the mean free path of electrons $l_e \approx 10^{-15} V_F = 3.5 \text{ \AA}$, which is comparable to the size of unit cell. Of course, this is a very small value corresponded to extremely “dirty” and disordered samples. In a previous study of $(\text{La}, \text{Nd})\text{H}_{10}$ ^[32] we found that the electron mean free path is also very short ($\approx 1.3 \text{ nm}$) and compatible with the unit cell parameter. This may lead to quantum effects of weak localization^[65] even in 3D samples of SnH_4 ,

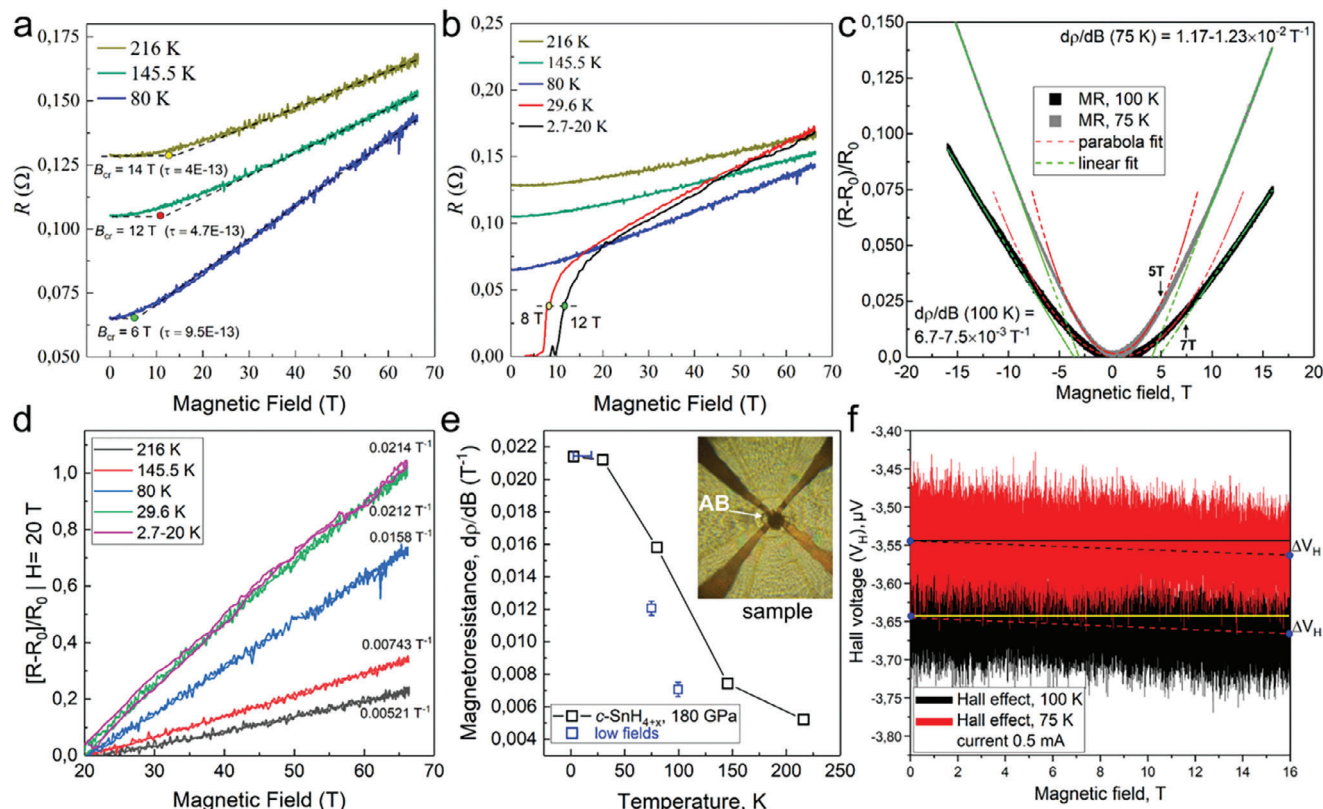


Figure 4. Magnetoresistance (MR) of the *fcc* SnH₄ at 180 GPa was measured in pulse magnetic fields. a) Dependence of the electrical resistance on the applied magnetic field at temperatures $T > T_C$. A pronounced transition from a quadratic to a linear $R(H_{ext})$ dependence is observed. b) Dependence of the sample resistance on the applied magnetic field over the entire temperature range. Due to the heating by eddy currents during the pulse, the sample temperature of 2.7 K cannot be considered reliably fixed. c) MR in low magnetic fields up to 16 T at temperatures 75 and 100 K. d) Linear part of the relative MR calculated for all temperature points starting from a field B_{ext} of 20 T. e) Dependence of linear MR on temperature. f) Attempt to measure the Hall effect in Sn hydrides at temperatures 75 and 100 K.

since the corresponding correction ($\delta\sigma$) to the electrical conductivity (σ) may be significant (Equation 3).

$$\frac{\delta\sigma}{\sigma} = -\frac{1}{k_F^2 l_e} \left(\frac{1}{l_e} - \frac{1}{l_\varphi} \right) \cong -1. \quad (3)$$

Weak localization effects are well known for semiconductors and graphene,^[66] in particular, they are responsible for the appearance of negative magnetoresistance in thin films of Si, Ge, and Te.^[67] A similar phenomenon was recently observed for (La,Nd)H₁₀, which exhibits a negative magnetoresistance in the range of 200–250 K.^[32] The weak localization can also lead to an unusual $R(T)$ dependence and sign reversal of dR/dT ,^[68] as it was observed for lanthanum-cerium (La,Ce)H₉ and sulfur H₃S hydrides (Figures S21c–22c, Supporting Information).

3. Discussion

Let us first discuss selection of the best theoretical structural model for *fcc* SnH₄ in terms of the experimental superconducting properties. The two predicted structures, namely *R3m*-Sn₁₂H₄₅ and *Fd3m*-Sn₈H₃₀, are dynamically stable, well describe the experimental powder XRD patterns, and lie near the convex hull

of Sn-H system (Figure S1, Supporting Information). They both have electronic band structures (Figure S11, Supporting Information) typical of metals. The low density of electronic states at the Fermi level (≈ 0.5 states per eV per Sn) also has a relatively weak contribution from the hydrogen atoms (half the contribution of Sn), which is usually attributed to low critical temperature of superconductivity.^[69,70] The calculated critical temperature for *Fd3m* modification ($T_C = 73$ –91 K, Figure S25, Supporting Information) is close to the experimental one (72–74 K) observed in *fcc* SnH₄ at 180 GPa. The results of single-crystal XRD, which do not reveal any deviations from the ideal *fcc* structure, as well as high critical temperature of superconductivity, indicate that only *Fd3m*-Sn₈H₃₀ theoretical model agrees well with the experimental data for *fcc* SnH₄ at 180 GPa.

It is now believed^[1] that hydrides belong to the conventional BCS superconductors and their behavior in the normal state can be described in terms of the Fermi liquid model, widely used for metals. However, gradually accumulating experimental data cast doubt on this point of view. First of all, it is necessary to note the change in the sign of the temperature coefficient of electrical resistance (dR/dT) from positive to negative along with decreasing pressure in DACs. This was observed in superconducting H₃S,^[1] PH_x,^[71] and lanthanum-cerium polyhydrides^[72] (Figure S20, Supporting Information). The decrease in electrical resistance with

increasing temperature is unusual for metals, but is a distinctive feature of insulators. Moreover, a similar behavior was recently observed in a cuprate superconductor Bi-2212 ($\text{Bi}_2\text{Sr}_2\text{CaCu}_2\text{O}_{8+x}$), studied at high pressures.^[73] This experiment demonstrated that pressure (P) may play the same role as the degree of doping (x),^[74,75] separating the superconducting phase from the pseudo-gap phase with an insulating-like negative dR/dT .

As many cuprates have a dome-shaped dependence of the critical $T_C(x)$ on the degree of doping (x), so do most superhydrides have a similar $T_C(P)$ dependence with a sharp decrease in T_C with pressure decreasing.^[1,2,6,7] Such decompression is usually accompanied by a sharp increase in the EPC parameter λ to the maximum within the Migdal-Eliashberg theory^[76,77] values of 3–3.7^[78] followed by decomposition of a compound. There is such a strong electron-phonon interaction that even a small shift of atoms causes a large change in the electronic structure, turning the metal into an insulator with local separation of charges (as in ferroelectrics) and formation of polarons.^[79] What can happen to the atomic sublattice of hydrogen in superhydrides under these conditions? It would be logical to assume that hydrogen atoms will form more stable H_2 molecules, and the compound will begin to exhibit the properties of a semiconductor, which is typical for molecular hydrides. That is exactly the boundary between the superconducting and insulating phases in polyhydrides.

The behavioral peculiarities of the electrical resistance of superhydrides have not received much attention since discovery of H_3S , but many of them (e.g., Figures S20–S21, Supporting Information) show $R(T)$ typical of strange metals in one pressure range, and the usual behavior of a Fermi liquid in another one. Amazingly, but the non-superconducting state of polyhydrides may turn out to be much closer to the properties of cuprate superconductors than previously thought, as Talantsev et al.^[80–83] predicted based on an analysis of the T_C/T_F ratio (T_F is the Fermi temperature).

4. Conclusions

We have synthesized a series of novel tin hydrides at a pressure of 180–210 GPa: $C2/m\text{-SnH}_{14}$, $fcc\text{-SnH}_4$, $fcc\text{-SnH}_{6+x}$, $fcc\text{-SnH}_2$, and $C2\text{-Sn}_{12}\text{H}_{18}$. The main product of the reaction of Sn with hydrogen at these pressures is the cubic (fcc) superconducting tetrahydride SnH_4 , with the composition being confirmed by XRD analysis performed after compression of cryogenically loaded stannane. The critical superconducting temperature of this compound is $T_C = 72\text{ K}$ at 180 GPa, the upper critical field is $B_{C2}(0) = 14\text{--}16\text{ T}$, the self-field critical current density is $J_C(0) \approx 8.8\text{ kA mm}^{-2}$, and the superconducting gap $2\Delta(0)$ is 21.6 meV. SnH_4 contains covalent Sn-H bonds, has soft modes in phonon spectra and the large electron-phonon coupling parameter $\lambda \approx 2.5$ due to important contribution of anharmonicity to the crystal lattice dynamics.

Another discovered polyhydride $C2/m\text{-SnH}_{14}$ with ultra-high hydrogen content, belongs to the same family of compounds as BaH_{12} ,^[34] LaH_{11-12} ,^[84] SrH_{22} ,^[30] and confirms the existence and prevalence of such a type of high molecular polyhydrides. Unlike other members of this group, SnH_{14} is expected to be a high-temperature superconductor with $T_C = 93\text{--}112\text{ K}$.

Tin tetrahydride (SnH_4) exhibits a reproducible anomalous dependence of electrical resistance on temperature, T -linear depen-

dence of the upper critical field, and a B -linear dependence of magnetoresistance over a wide range of magnetic fields and temperatures. Such a non-Fermi-liquid behavior is reminiscent to the unconventional non-superconducting state of cuprate high-temperature superconductors.

Supporting Information

Supporting Information is available from the Wiley Online Library or from the author.

Acknowledgements

In situ X-ray diffraction experiments at high pressure were performed on ESRF, stations ID 18 and ID 27, Grenoble, France (proposal No. HC-2902, 2017), as well as on PETRA III, beamline P02.2, Hamburg, Germany (2020), and at HPCAT (sector 16) of the APS, Argonne National Laboratory. HPCAT operations are supported by the U.S. Department of Energy (DOE) National Nuclear Security Administration's Office of Experimental Sciences. The APS is a DOE Office of Science User Facility operated for the DOE Office of Science by Argonne National Laboratory under Contract No. DE-AC02-06CH11357. A.F.G. acknowledges the support from NSF CHE 2302437. Experiments in pulsed magnetic fields were done in Dresden High Magnetic Field Laboratory (HLD HZDR), Dresden, Germany (2021). This work was supported by HLD-HZDR, member of the European Magnetic Field Laboratory (EMFL). The high-pressure experiments were supported by the Ministry of Science and Higher Education of the Russian Federation within the state assignment of the FSRC Crystallography and Photonics of the RAS and by the Russian Science Foundation (Project No. 22-12-00163). I.A.K. thanks the Russian Science Foundation (grant No. 21-73-10261) for the financial support of the anharmonic phonon density of states calculations and molecular dynamics simulations. SEM, XRF, and XRD studies of the initial alloys were performed using the equipment of the Shared Research Center FSRC Crystallography and Photonics of the RAS. I.A.T. and A.G.I. acknowledge the use of the facilities of the Center for Collective Use "Accelerator Center for Neutron Research of the Structure of Substance and Nuclear Medicine" of the INR RAS for high-pressure cell preparation. The research used resources of the LPI Shared Facility Center. V.M.P., A.V.S., and O.A.S. acknowledge the support of the state assignment of the Ministry of Science and Higher Education of the Russian Federation (Project No. 0023-2019-0005) and the Russian Science Foundation, grant 22-22-00570. I.A.K. thanks the Russian Science Foundation (grant No. 21-73-10261) for the financial support of the development of T-USPEX method and anharmonic phonon density of states calculation algorithm. S.W.T. was supported by NSF Cooperative Agreement No. DMR-1157490/1644779 and by the State of Florida. The authors acknowledge the support of the HLD at HZDR, member of the European Magnetic Field Laboratory (EMFL). The authors also thank Dr. E. Talantsev (IMP RAS) for calculations within two-gap models, and Prof. Artem R. Oganov for help in using the USPEX code.

Conflict of Interest

The authors declare no conflict of interest.

Author Contributions

I.A.T., D.V.S., and A.G.I. contributed equally to this work. I.A.T., D.V.S., D.Z., T.H., and S.W.T. performed the experiments. I.A.K. performed the T-USPEX and anharmonic phonon density of states calculations. A.G.K., D.V.S., and D.Z. prepared the theoretical analysis and calculated the equation of states, electron and phonon band structures, and superconducting

properties of tin hydrides. D.V.S. and D.Z. analyzed and interpreted the experimental results and wrote the manuscript. I.A.T., A.V.S., and O.A.S. made the electric transport measurements in low magnetic fields. M.V.L. analyzed Raman experiments and edited the manuscript. D.S.P. built a system for the synthesis and cryogenic loading of stannane. T.H. and S.W.T. carried out the measurements in pulsed magnetic fields at HZDR HLD. I.S.L. and V.M.P. directed the research, analyzed the results and edited the manuscript. All the authors provided critical feedback and helped shape the research.

Data Availability Statement

The data that support the findings of this study are available in the supplementary material of this article.

Keywords

high pressure, non-Fermi-liquid, superconductivity, tin hydrides

Received: June 3, 2023

Revised: July 18, 2023

Published online:

- [1] A. P. Drozdov, M. I. Erements, I. A. Troyan, V. Ksenofontov, S. I. Shylin, *Nature* **2015**, 525, 73.
- [2] A. P. Drozdov, P. P. Kong, V. S. Minkov, S. P. Besedin, M. A. Kuzovnikov, S. Mozaffari, L. Balicas, F. F. Balakirev, D. E. Graf, V. B. Prakapenka, E. Greenberg, D. A. Knyazev, M. Tkacz, M. I. Erements, *Nature* **2019**, 569, 528.
- [3] M. Somayazulu, M. Ahart, A. K. Mishra, Z. M. Geballe, M. Baldini, Y. Meng, V. V. Struzhkin, R. J. Hemley, *Phys. Rev. Lett.* **2019**, 122, 027001.
- [4] D. V. Semenok, A. G. Kvashnin, A. G. Ivanova, V. Svitlyk, V. Y. Fominski, A. V. Sadakov, O. A. Sobolevskiy, V. M. Pudalov, I. A. Troyan, A. R. Oganov, *Mater. Today* **2020**, 33, 36.
- [5] I. A. Troyan, D. V. Semenok, A. G. Kvashnin, A. V. Sadakov, O. A. Sobolevskiy, V. M. Pudalov, A. G. Ivanova, V. B. Prakapenka, E. Greenberg, A. G. Gavriluk, I. S. Lyubutin, V. V. Struzhkin, A. Bergara, I. Errea, R. Bianco, M. Calandra, F. Mauri, L. Monacelli, R. Akashi, A. R. Oganov, *Adv. Mater.* **2021**, 33, 2006832.
- [6] P. Kong, V. S. Minkov, M. A. Kuzovnikov, A. P. Drozdov, S. P. Besedin, S. Mozaffari, L. Balicas, F. F. Balakirev, V. B. Prakapenka, S. Chariton, D. A. Knyazev, E. Greenberg, M. I. Erements, *Nat. Commun.* **2021**, 12, 5075.
- [7] W. Chen, D. V. Semenok, X. Huang, H. Shu, X. Li, D. Duan, T. Cui, A. R. Oganov, *Phys. Rev. Lett.* **2021**, 127, 117001.
- [8] L. Ma, K. Wang, Y. Xie, X. Yang, Y. Wang, M. Zhou, H. Liu, X. Yu, Y. Zhao, H. Wang, G. Liu, Y. Ma, *Phys. Rev. Lett.* **2022**, 128, 167001.
- [9] Z. Li, X. He, C. Zhang, X. Wang, S. Zhang, Y. Jia, S. Feng, K. Lu, J. Zhao, J. Zhang, B. Min, Y. Long, R. Yu, L. Wang, M. Ye, Z. Zhang, V. Prakapenka, S. Chariton, P. A. Ginsberg, J. Bass, S. Yuan, H. Liu, C. Jin, *Nat. Commun.* **2022**, 13, 2863.
- [10] D. V. Semenok, I. A. Kruglov, I. A. Savkin, A. G. Kvashnin, A. R. Oganov, *Curr. Opin. Solid State Mater. Sci.* **2020**, 24, 100808.
- [11] A. S. Naumova, S. V. Lepeshkin, A. R. Oganov, *J. Phys. Chem. C* **2019**, 123, 20497.
- [12] T. Yang, J. Liu, X. Liu, X. Liu, N. Li, *Crystals* **2021**, 11, 1499.
- [13] D. Duan, Y. Liu, Y. Ma, Z. Shao, B. Liu, T. Cui, *National Science Review* **2017**, 4, 121.
- [14] T. A. Strobel, M. Somayazulu, R. J. Hemley, *Phys. Rev. Lett.* **2009**, 103, 065701.
- [15] S. Wang, H.-k. Mao, X.-J. Chen, W. L. Mao, *Proc. Natl. Acad. Sci. USA* **2009**, 106, 14763.
- [16] P. P. Kong, A. P. Drozdov, E. Eroke, M. I. Erements, presented at Book of abstracts of AIRAPT 26 joint with ACHPR 8 & CHPC 19, Pressure-induced superconductivity above 79 K in Si₂H₆, Beijing **2017**.
- [17] M. M. Davari Esfahani, A. R. Oganov, H. Niu, J. Zhang, *Phys. Rev. B* **2017**, 95, 134506.
- [18] T. A. Strobel, X.-J. Chen, M. Somayazulu, R. J. Hemley, *J. Chem. Phys.* **2010**, 133, 164512.
- [19] G. Zhong, C. Zhang, X. Chen, Y. Li, R. Zhang, H. Lin, *J. Phys. Chem. C* **2012**, 116, 5225.
- [20] G. Gao, A. R. Oganov, P. Li, Z. Li, H. Wang, T. Cui, Y. Ma, A. Bergara, A. O. Lyakhov, T. Iitaka, G. Zou, *Proc. Natl. Acad. Sci. USA* **2010**, 107, 1317.
- [21] B. Chen, L. J. Conway, W. Sun, X. Kuang, C. Lu, A. Hermann, *Phys. Rev. B* **2021**, 103, 035131.
- [22] Y. Cheng, C. Zhang, T. Wang, G. Zhong, C. Yang, X.-J. Chen, H.-Q. Lin, *Sci. Rep.* **2015**, 5, 16475.
- [23] P. Zaleski-Eggier, R. Hoffmann, N. W. Ashcroft, *Phys. Rev. Lett.* **2011**, 107, 037002.
- [24] B. Guigue, P. Loubeyre, *J. Appl. Phys.* **2021**, 129, 225901.
- [25] F. Hong, P. F. Shan, L. X. Yang, B. B. Yue, P. T. Yang, Z. Y. Liu, J. P. Sun, J. H. Dai, H. Yu, Y. Y. Yin, X. H. Yu, J. G. Cheng, Z. X. Zhao, *Mater. Today Phys.* **2022**, 22, 100596.
- [26] C. Ritter, J. Synthesis of stannane and deuterostannane. the US patent WO/2012/021634 **2012**.
- [27] A. G. Gavriluk, I. A. Troyan, A. G. Ivanova, S. N. Aksenov, S. S. Starchikov, I. S. Lyubutin, W. Morgenroth, K. V. Glazyrin, M. Mezouar, *JETP Lett.* **2017**, 106, 733.
- [28] A. Salamat, G. Garbarino, A. Dewaele, P. Bouvier, S. Petitgirard, C. J. Pickard, P. F. McMillan, M. Mezouar, *Phys. Rev. B* **2011**, 84, 140104.
- [29] M. M. D. Esfahani, Z. Wang, A. R. Oganov, H. Dong, Q. Zhu, S. Wang, M. S. Rakitin, X. Zhou, *Sci. Rep.* **2016**, 6, 22873.
- [30] D. V. Semenok, W. Chen, X. Huang, D. Zhou, I. A. Kruglov, A. B. Mazitov, M. Galasso, C. Tantardini, X. Gonze, A. G. Kvashnin, A. R. Oganov, T. Cui, *Adv. Mater.* **2022**, 34, 2200924.
- [31] J. E. Hirsch, F. Marsiglio, *Phys. Rev. B* **2021**, 103, 134505.
- [32] D. V. Semenok, I. A. Troyan, A. V. Sadakov, D. Zhou, M. Galasso, A. G. Kvashnin, A. G. Ivanova, I. A. Kruglov, A. A. Bykov, K. Y. Terent'ev, A. V. Cherepakhin, O. A. Sobolevskiy, K. S. Pervakov, A. Y. Seregina, T. Helm, T. Förster, A. D. Grockowiak, S. W. Tozer, Y. Nakamoto, K. Shimizu, V. M. Pudalov, I. S. Lyubutin, A. R. Oganov, *Adv. Mater.* **2022**, 34, 2204038.
- [33] D. V. Semenok, I. A. Troyan, A. G. Kvashnin, A. G. Ivanova, M. Hanfland, A. V. Sadakov, O. A. Sobolevskiy, K. S. Pervakov, A. G. Gavriluk, I. S. Lyubutin, K. Glazyrin, N. Giordano, D. Karimov, A. Vasiliev, R. Akashi, V. M. Pudalov, A. R. Oganov, *Mater. Today* **2021**, 48, 18.
- [34] W. Chen, D. V. Semenok, A. G. Kvashnin, X. Huang, I. A. Kruglov, M. Galasso, H. Song, D. Duan, A. F. Goncharov, V. B. Prakapenka, A. R. Oganov, T. Cui, *Nat. Commun.* **2021**, 12, 273.
- [35] D. Sun, V. S. Minkov, S. Mozaffari, Y. Sun, Y. Ma, S. Chariton, V. B. Prakapenka, M. I. Erements, L. Balicas, F. F. Balakirev, *Nat. Commun.* **2021**, 12, 6863.
- [36] G. Seibold, R. Arpaia, Y. Y. Peng, R. Fumagalli, L. Braicovich, C. Di Castro, M. Grilli, G. C. Ghiringhelli, S. Caprara, *Commun. Phys.* **2021**, 4, 7.
- [37] F. Bloch, *Z. Physik* **1930**, 59, 208.
- [38] J. Bardeen, L. N. Cooper, J. R. Schrieffer, *Phys. Rev.* **1957**, 108, 1175.
- [39] N. R. Werthamer, E. Helfand, P. C. Hohenberg, *Phys. Rev.* **1966**, 147, 295.
- [40] I. Osmond, J. Buhot, presented at Conference on Science at Extreme Conditions, oral reports, **2021**.
- [41] F. Hunte, J. Jaroszyński, A. Gurevich, D. C. Larbalestier, R. Jin, A. S. Sefat, M. A. McGuire, B. C. Sales, D. K. Christen, D. Mandrus, *Nature* **2008**, 453, 903.

- [42] H. Q. Yuan, J. Singleton, F. F. Balakirev, S. A. Baily, G. F. Chen, J. L. Luo, N. L. Wang, *Nature* **2009**, 457, 565.
- [43] V. A. Gasparov, N. S. Sidorov, I. I. Zver'kova, *Phys. Rev. B* **2006**, 73, 094510.
- [44] S. Khim, B. Lee, J. W. Kim, E. S. Choi, G. R. Stewart, K. H. Kim, *Phys. Rev. B* **2011**, 84, 104502.
- [45] C. Wang, S. Yi, J.-H. Cho, *Phys. Rev. B* **2020**, 101, 104506.
- [46] K. Kuroki, T. Higashida, R. Arita, *Phys. Rev. B* **2005**, 72, 212509.
- [47] D. Semenok, *Computational design of new superconducting materials and their targeted experimental synthesis Doctoral program in materials science and engineering thesis*, Skoltech, Moscow, Russia **2022**.
- [48] H. Jeon, C. Wang, S. Liu, J. M. Bok, Y. Bang, J.-H. Cho, *New J. Phys.* **2022**, 24, 083048.
- [49] B. Spivak, F. Zhou, *Phys. Rev. Lett.* **1995**, 74, 2800.
- [50] V. M. Galitski, A. I. Larkin, *Phys. Rev. Lett.* **2001**, 87, 087001.
- [51] E. F. Talantsev, J. L. Tallon, *Nat. Commun.* **2015**, 6, 7820.
- [52] E. Talantsev, W. P. Crump, J. L. Tallon, *Ann. Phys.* **2017**, 529, 1700197.
- [53] J. Hu, T. F. Rosenbaum, *Nat. Mater.* **2008**, 7, 697.
- [54] N. N. Klimov, D. A. Knyazev, O. E. Omel'yanovskii, V. M. Pudalov, H. Kojima, M. E. Gershenson, *Phys. Rev. B* **2008**, 78, 195308.
- [55] Y. A. DREIZIN, A. M. DYKHNE, *Sov. Phys. JETP* **1973**, 36, 127.
- [56] A. M. Dykhne, *Sov. Phys. JETP* **1971**, 32, 63.
- [57] P. V. Gorskii, *Physica i Technika poluprovodnikov* **2004**, 38, 864.
- [58] C. Boyd, P. W. Phillips, *Phys. Rev. B* **2019**, 100, 155139.
- [59] A. Legros, S. Benhabib, W. Tabis, F. Laliberté, M. Dion, M. Lizaire, B. Vignolle, D. Vignolles, H. Raffy, Z. Z. Li, P. Auban-Senzier, N. Doiron-Leyraud, P. Fournier, D. Colson, L. Taillefer, C. Proust, *Nat. Phys.* **2019**, 15, 142.
- [60] A. Ataei, A. Gourgout, G. Grissonnanche, L. Chen, J. Baglo, M. E. Boulanger, F. Laliberté, S. Badoux, N. Doiron-Leyraud, V. Oliviero, S. Benhabib, D. Vignolles, J. S. Zhou, S. Ono, H. Takagi, C. Proust, L. Taillefer, *Nat. Phys.* **2022**, 18, 1420.
- [61] R. L. Greene, P. R. Mandal, N. R. Poniatowski, T. Sarkar, *Annu. Rev. Condens. Matter Phys.* **2020**, 11, 213.
- [62] E. F. Talantsev, *Matter and Radiation at Extremes* **2022**, 7, 058403.
- [63] P. Drude, *Ann. Phys.* **1900**, 306, 566.
- [64] P. Drude, *Ann. Phys.* **1900**, 308, 369.
- [65] B. L. Altshuler, A. G. Aronov, A. I. Larkin, D. E. Khmel'nitskil, *Zh. Eksp. Teor. Fiz.* **1981**, 81, 768.
- [66] F. V. Tikhonenko, D. W. Horsell, R. V. Gorbachev, A. K. Savchenko, *Phys. Rev. Lett.* **2008**, 100, 056802.
- [67] H. Mell, J. Stuke, *J. Non-Cryst. Solids* **1970**, 4, 304.
- [68] L. Van den dries, C. Van Haesendonck, Y. Bruynseraede, G. Deutscher, *Phys. Rev. Lett.* **1981**, 46, 565.
- [69] J. Appel, *Phys. Rev. B* **1976**, 13, 3203.
- [70] F. Belli, T. Novoa, J. Contreras-García, I. Errea, *Nat. Commun.* **2021**, 12, 5381.
- [71] A. P. Drozdov, M. I. Erements, I. A. Troyan, arXiv:1508.06224, **2015**.
- [72] W. Chen, X. Huang, D. V. Semenok, S. Chen, D. Zhou, K. Zhang, A. R. Oganov, T. Cui, *Nat. Commun.* **2023**, 14, 2660.
- [73] Y. Zhou, J. Guo, S. Cai, J. Zhao, G. Gu, C. Lin, H. Yan, C. Huang, C. Yang, S. Long, Y. Gong, Y. Li, X. Li, Q. Wu, J. Hu, X. Zhou, T. Xiang, L. Sun, *Nat. Phys.* **2022**, 18, 406.
- [74] C. W. Chu, L. Z. Deng, B. Lv, *Phys. C (Amsterdam, Neth.)* **2015**, 514, 290.
- [75] P. A. Lee, N. Nagaosa, X.-G. Wen, *Rev. Mod. Phys.* **2006**, 78, 17.
- [76] G. M. Eliashberg, *Sov. Phys. JETP* **1959**, 11, 696.
- [77] A. B. Migdal, *Sov. Phys. JETP* **1958**, 34, 996.
- [78] E. A. Yuzbashyan, B. L. Altshuler, *Phys. Rev. B* **2022**, 106, 054518.
- [79] A. S. Alexandrov, A. B. Krebs, *Sov. Phys. Usp.* **1992**, 35, 345.
- [80] E. F. Talantsev, R. C. Mataira, *Mater. Res. Express* **2020**, 7, 016003.
- [81] E. F. Talantsev, *Supercond. Sci. Technol.* **2020**, 33, 124001.
- [82] E. F. Talantsev, *Materials (Basel)* **2021**, 14, 4322.
- [83] E. F. Talantsev, *Results in Physics* **2020**, 16, 102993.
- [84] M. A. Kuzovnikov, presented at ELBRUS2021, V(P) equations of state of novel lanthanum and yttrium superhydrides, **2021**.